[**Article ID**] 1003 - 6326(2002) 06 - 1081 - 06

Thermal activation approaches to deformation mechanisms for high Nb containing TiAl base alloys ¹⁰

LIU Zircheng(刘自成), WANG Yan-li(王艳丽), LIN Jumpin(林均品), ZHANG Weirjun(张卫军), CHEN Guorliang(陈国良) (State Key laboratory for Advanced Metals and Materials, University of Science and Technology Beijing, Beijing 100083, China)

[Abstract] The deformation mechanisms in a wide temperature range from room temperature to 1 200 K were investigated by thermal activation approach. Using observed instantaneous stress response to the strain rate jump (Δ^{G}_{tr}), the activation volume V_a , then the activation enthalpy ΔH , activation free enthalpy ΔG and activation entropy ΔS were calculated. The apparent activation energy of high temperature deformation is estimated to be 3.66 eV, which is larger than the self-diffusion coefficient of binary TiAl (3.01 eV). The dislocations at 1 173 K are generally curved or bowed, even helical shaped dislocations. The climb of ordinary dislocations as well as twinning has greatly contributed to the plastic deformation. The CRSS at 1 173 K is estimated to be 180 MPa. The higher resisting stress at both room temperature and elevated temperature might relate to the high Nb content of the alloy.

[Key words] TiAl; thermal activation approach; deformation mechanisms

[CLC number] TG 146

[Document code] A

1 INTRODUCTION

In recent years, significant progress has been obtained in improving individual mechanical properties mainly by alloying with ternary element and controlling the microstructures in a dual phase Y-TiAl. Nevertheless, the low ambient ductility, fracture toughness and high temperature strength are often inappropriately balanced^[1, 2]. These properties can be related to the dislocation mechanisms operating under the respective deformation conditions. Understanding these mechanisms can give valuable information for optimizing the mechanical properties. Some researchers have analyzed the deformation mechanism in dual phase TiAl alloys by thermal activation theory^[3, 4].

Kim^[5] has indicated that high Nb containing TiAl base alloy developed by Chen et al^[6~8] is the first example for the development of high temperature high performance TiAl alloy. The high Nb containing TiAl alloy exhibits very high strength at both room temperature and high temperature^[7]. The systematic study of the deformation behavior for high Nb containing TiAl alloy is not reported. The present study is to characterize the deformation mechanisms of high Nb containing TiAl based alloys by thermal activation theory. The work has been carried out on the Tr45Al-10Nb alloy with near fully lamellar microstructure and the analysis is based on the results of compressive experiments with a wide temperature range. The results will be compared with those obtained from ordinary TiAl-based alloys, which is current-

ly being considered for high temperature structural applications.

2 FUNDAMENTAL OF THERMAL ACTIVA-TION APPROACH OF DEFORMATION BE-HAVIOR

The thermal activation approach is a useful means to explore the plastic deformation behavior, particularly rate related deformation behavior at high temperature. Schock^[9] and Gibbbs have suggested the fundamental of the thermal activation approach of deformation behavior.

According to the thermal activation approach, the strain rate $\dot{\epsilon}$ equation can be written as follows [10]:

$$\dot{\mathbf{E}} = \dot{\mathbf{E}}_0 \exp(-\Delta G/kT)$$
 (1)

$$\Delta G = \Delta F - V_{\rm a} T^* \tag{2}$$

$$T = T_{\mu} + T^* \tag{3}$$

where ΔG is Gibbs free energy of thermal activation; k is the Boltzmann constant and $\dot{\epsilon}_0$ is a rate constant; ΔF is Helmholtz free energy of thermal activation, which describes the total energy needed to overcome the obstacles at given $\dot{\epsilon}$, T and applied stress τ ; V_a is activation volume, and $V_a = lb \Delta R$, where l is the obstacle distance, b is the Burgers vector, and ΔR is the obstacle diameter. The energy contribution $V_a \tau^*$ is the mechanical work done by the applied stress τ during glide deformation. τ^* is called effective stress, which is the thermal part of the resisting stress to dislocation glide that can be overcome by thermal activation. τ_μ is ather-

mal part of the resisting stress to glide dislocation, which must be overcome by applied stress. T_{μ} is the athermal long-range resisting stress component. In general, the athermal long-range resisting stress component inside single phase is independent of temperature apart from a small chance due to temperature dependence of shear modulus(μ) in a temperature range close to room temperature in which the dislocation arrangements of deformed specimens are similar.

The following equations were used to calculate the corresponding activation parameters^[9,11]:

$$V_{\rm a} = fkT \left(\Delta \ln \mathcal{E} / \Delta \sigma_{\rm tr} \right)_T \tag{4}$$

$$Q_{\text{app.}} = \Delta H = -TV_{\delta} f^{-1} (\Delta \mathcal{O}/\Delta T) \epsilon$$
 (5)

$$\Delta G = \frac{\Delta H + \frac{V_{\rm a} \sigma}{f} \bullet \frac{\partial (\ln \mu)}{\partial (\ln T)}}{1 - \frac{\partial (\ln \mu)}{\partial (\ln T)}}$$
(6)

$$\Delta S = \frac{\Delta H - \Delta G}{T} = -\frac{\frac{\partial (\ln \mu)}{\partial T}}{1 - \frac{\partial (\ln \mu)}{\partial (\ln T)}} \left[\Delta H + \frac{V_a \sigma}{f} \right]$$
(7)

where V_a is activation volume; ΔH and ΔS are activation enthalpy and activation entropy respectively; T and $\dot{\epsilon}$ are absolute temperature and strain rate; σ is flow stress; μ is the shear modulus (GPa); k is Boltzmann constant; and Taylor factor f is equal to 3. Assume the relationship between the shear modulus and temperature is similar to that of single phase of TiAl:

$$\mu$$
= 72. 24- 0. 014 1 T (8)

3 EXPERIMENTAL

The alloy of nominal composition (mole fraction, %) of Tr 45Al-10Nb was produced by vacuum induction melting furnace with cold copper crucible. The oxygen content of the alloys is analyzed to be 7. 80×10^{-4} . After the isothermal forging, the cylindrical specimens with dimensions of d 5 mm × 10 mm are heat-treated at 1 578 K for 30 min, then directly transferred to 1 173 K for 30 min and air cooled. The microstructure is identified as nearly full lamellar(NL) shown in Fig. 1. The volume fraction of fine grains (dark) and β phase (light) on the colony boundaries are approximately 10% and < 1%, respectively. The identification of the phases was conducted by TEM because the phases have different compositions. The colony size is about 90 μ m, and the volume fraction of α_2 is close to 15%, which was measured by the point count metallographic method with an accuracy of $1\% \sim 2\%$.

Compressive tests were performed on Geeble1500 simulation machine at 298, 398, 523, 673, 823, 973, 1 033, 1 088, 1 173 and 1 273 K with a strain rate of 5 \times 10⁻⁴ s⁻¹ and immediately followed by water

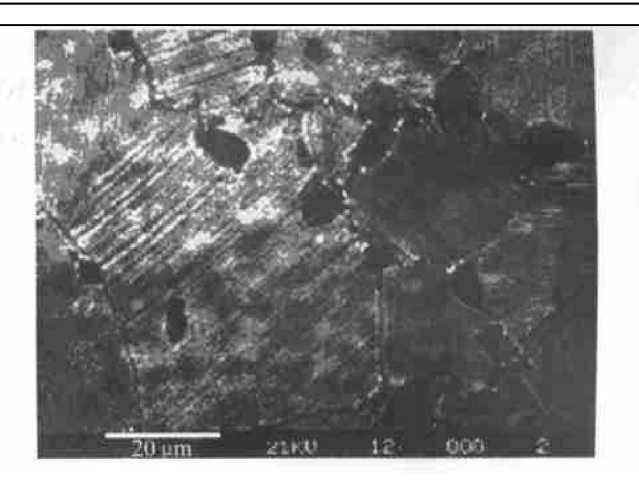


Fig. 1 SEM photograph of NL microstructures of Ti45Al10Nb alloy

quenching. Strain rate jump tests for the measurement of strain rate sensitive coefficient of certain microstructure, ($\Delta \sigma_{\rm tr}/\ln \dot{\epsilon}$)_T, were conducted at the yield point by instantaneously jumping the strain rate from 5×10^{-3} s⁻¹ to 5×10^{-2} s⁻¹. The observed data of ($\Delta \sigma_{\rm tr}/\ln \dot{\epsilon}$)_T were used to calculate the activation volume of the glide deformation. Thin foils for TEM observations were cut parallel to the compressive axis from the specimens deformed to a strain of 3%, and then jet polished in a solution of 7% sulfur acid + 93% methanol at - 20 °C and 15 V. TEM observations were carried out using H-800 and Philips EM-400T transmission electron microscopes.

4 RESULTS

4. 1 Temperature dependence of yield strength

The temperature dependence of yield strength $\sigma_{0.2}$ from room temperature to 1 273 K at the strain rates of $5\times 10^{-3}~{\rm s}^{-1}$ and $5\times 10^{-4}~{\rm s}^{-3}$ are shown in Fig. 2. The temperature dependence of $\sigma_{0.2}$ could be divided into three different regions. In the temperature range close to room temperature ($298\sim 523~{\rm K}$), the strength $\sigma_{0.2}$ slightly decreases with increasing temperature and decreasing strain rate. This implies that the deformation in

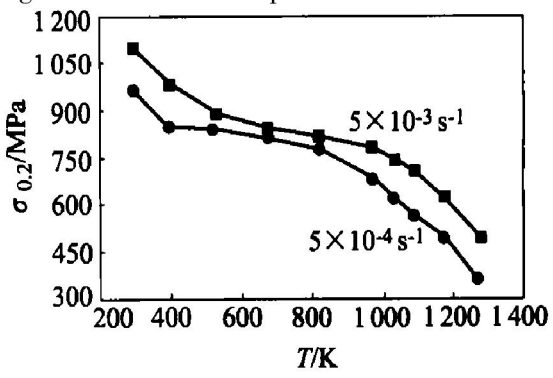


Fig. 2 Temperature dependence of yield strength on high Nb containing TiAl alloy

the temperature region may be related to thermal activation. In the elevated temperature region ($523\sim1~033~K$), $\sigma_{0.2}$ exhibits almost temperature independence. That is attributed to the insensitivity or low sensitivity of the flow stress to the temperature. The slightly apparent change in the yield strength with temperature is due to the temperature dependence of the shear modulus. In the high temperature region ($1~033\sim1~273~K$), $\sigma_{0.2}$ is greatly sensitive to the temperature and the strain rate. Obviously, it is because that the high temperature plastic deformation should be thermal activity. The transition temperature for the significant decrease in yield strength decreases with decreasing strain rate.

4. 2 Calculation of activation volume and thermodynamic parameters

The observed instantaneous stress response to the strain rate jump($\Delta \sigma_{\rm tr}$) is measured and shown in Table 1. Then, the activation volume $V_{\rm a}$, could be calculated by substituting observed data of $\Delta \sigma_{\rm tr}$ into equation (4). $V_{\rm a}$ is presented in the unit of b^3 , where b is the Burgers vector of 1/2 \langle 110] ordinary dislocation. The choice does not mean that only 1/2 \langle 110] ordinary dislocation is activated in the investigated temperature range. Indeed, the 1/2 \langle 110] ordinary dislocation is the main moving dislocation. Substituting the observed data of activation volume into equations (1) \sim (5), the activation enthalpy ΔH , activation free enthalpy ΔG and activation entropy ΔS can be further calculated as listed in Table 1 and plotted in Fig. 3.

Table 1 Observed and calculated data of $\Delta \sigma_{tr}$, activation volume V_a , activation enthalpy ΔH , activation free energy ΔG and activation entropy ΔS (strain rate = $5 \times 10^{-3} \text{ s}^{-1}$)

entropy ΔS (strain rate = $3 \times 10^{\circ}$ s)						
Temp. /	σ _{0. 2} / MPa	Δσ _{tr} / MPa	$V_{\rm a}$ (b^3)	Δ <i>H</i> / eV	$\Delta G / \mathrm{eV}$	$\Delta S/$ (eV•K ⁻¹)
298	1 101	24. 5	51. 1	0. 88	0. 68	6. 72 × 10 ⁻⁴
398	978	27.5	60.8	0.79	0.52	6.83×10^{-4}
523	891	9.7	225.3	1. 92	0.79	2.16×10^{-3}
673	839	5.8	488.6	2. 57	0. 23	4. 16×10^{-3}
823	812	6. 1	566.7	4. 25	0. 19	4.93×10^{-3}
973	783	19	215.6	7.46	4. 61	2.93×10^{-3}
1 033	738	32. 2	134. 2	4. 52	2.71	1.75×10^{-3}
1 088	700	38. 2	78.5	3. 74	2.43	1.20×10^{-3}
1 173	621	97. 2	50.7	3.68	2.53	9.81×10^{-4}
1 273	490	118	45.3	3. 58	2.46	8.79×10^{-4}

The activation free energy ΔG could be roughly divided into three catalogs. The data of ΔG in the high temperature is very high, corresponding to the strong temperature dependence of the yield strength. At elevat-

ed temperature range (673~ 823 K), ΔG is the smallest that implies the athermal property of the glide deformation, and corresponding to the temperature independent of the yield strength. It should be emphasized that ΔG in the temperature range of 298~ 398 K is relatively larger that indicates possibly temperature dependence of yield strength, which has been illustrated by the observed data of yield stress.

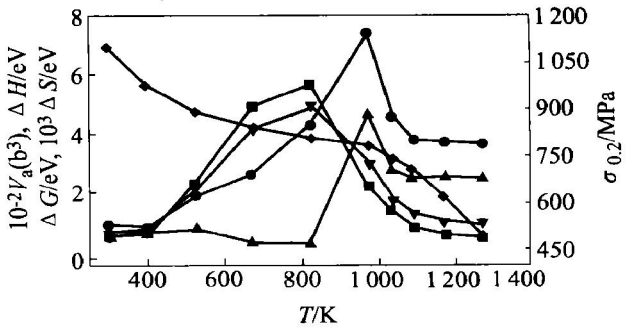


Fig. 3 Temperature dependence of $G_{0.2}$, V_{a} , ΔH , ΔG and ΔS , $G_{0.2}$

Correspondingly, there are two transition temperature ranges among these three temperature catalogs in the ΔG and ΔH curves, which are consistent to the transition behavior in the yield stress vs temperature curves.

4. 3 Calculation of effective stress τ^*

Equation (2) can be differentiated by
$$T$$
:
$$\begin{bmatrix} \frac{\partial \Delta G}{\partial T} \end{bmatrix}_{\tau^*} = \begin{bmatrix} \frac{\partial \Delta F}{\partial T} \end{bmatrix}_{\tau^*} - \tau^* \begin{bmatrix} \frac{\partial V_a}{\partial T} \end{bmatrix}_{\tau^*}$$
(9)

Because of that the deformation mechanisms could not be changed as the deformation temperature changes from 298 K to 389 K, ΔF can be assumed to be unchanged, i. e. $[(\partial \Delta F)/(\partial T)]_{\tau^*} = 0$, then equation (9) can be rewritten as follows:

be rewritten as follows:
$$\begin{bmatrix} \frac{\partial \triangle G}{\partial T} \end{bmatrix}_{\tau^*} = - \tau^* \begin{bmatrix} \frac{\partial V_a}{\partial T} \end{bmatrix}_{\tau^*}$$
 (10)

Assuming the athermal resisting part of the dislocation glide τ_{μ} is unchanged in the range of 298~ 398 K. Equation (10) can be transferred to:

$$\begin{bmatrix} \frac{\partial \Delta G}{\partial T} \end{bmatrix}_{\dot{\mathbf{E}}} = - \tau^* \begin{bmatrix} \frac{\partial V_a}{\partial T} \end{bmatrix}_{\dot{\mathbf{E}}} \tag{11}$$

Or approximately written in a limited temperature range (298~398 K) and a constant strain rate:

$$\frac{\Delta G_{1} - \Delta G_{2}}{T_{1} - T_{2}} = - \tau^{*} \left[\frac{V_{a1} - V_{a2}}{T_{1} - T_{2}} \right]$$
 (12)

Taking the data of ΔG and V_a shown in Table 1 and $b = 2.83 \times 10^{-10}$ m, T^* at 298 K and strain rate of 5×10^{-3} s⁻¹ can be calculated to be 117 MPa, and therefore $T_{\mu}(298 \text{ K})$ can be further calculated to be 250 MPa by using Eqn. (3). Similarly, T^* (398 K) = 81 MPa, and $T_{\mu}(398 \text{ K}) = 245 \text{ MPa}$.

The athermal long-range resisting stress τ_{μ} of moving dislocations can be composed of three parts: resisting stresses caused by lamellar interfaces, colony boundaries

and elastic interaction with dislocation forest inside Y grain or lath, i. e.

$$T_{\mu} = T_{\lambda} + T_{d} + T_{dis} \tag{13}$$

The resisting stresses caused by both lamellar interfaces(τ_{λ}) and colony boundary(τ_{d}) could be estimated to be 146. 7 MPa and 37. 3 MPa, respectively, by using the data of k_{λ} (~ 0. 22 MPa) [10] and $k_{\rm d}$ (1. 0 MPa $\sqrt{m}\,)^{\,[\,5,\ 12\,]}$ and the observed lamellar spacing ($0.\ 25$ 14m) and colony size (80 14m) of the alloy. Therefore, the resisting stress from the athermal long-range elastic interaction with dislocation $T_{\rm dis}(298 \text{ K}) = 66 \text{ MPa}$. These data indicate that the resisting stress from the interfaces (184 MPa) accounts for the main part of the athermal long-range resisting stress. The resisting stress from the athernal long-range elastic interaction with dislocation forest inside grain T_{dis} accounts for about 1/4 of the total athermal resisting stress.

According to the generally accepted assumption, $\sigma_{\mu} = 3 \, \tau_{\mu} \propto \mu(\mathit{T})$, and the linear temperature dependence of $\mu(\mathit{T})$ expressed by Eqn. (8), the relationship between σ_{μ} and T can be considered to be linear in a temperature range in which the dislocation arrangements of deformed specimens are similar. Then, the decrease of σ_{μ} should be proportional to the increase of temperature:

$$\sigma_{\mu} = \sigma_0 + \sigma T$$
 (14)

where σ_0 and α could be estimated from equation (8) and by substituting σ_{μ} = 750 MPa at 298 K into equation. (14). Then,

$$\sigma_{\mu} = 795 - 0.151T (MPa)$$
 (15)

Using eqn. (15) σ_{μ} at various temperatures (523 ~ 973 K) could be estimated. then τ^* can be further calculated by Eqn. (3), shown as Table 2.

Table 2 Calculated σ_μ and τ* at

various temperatures								
Temp. / K	$T_{0.2}/MPa$	$\tau_{\mu}/M\mathrm{Pa}$	τ* / MPa					
298	367	250	117					
398	326	245	81					
523	297	239	58					
673	280	231	49					
823	271	224	47					
973	261	216	45					

Table 2 indicates that the effective stress τ^* decreases with increasing temperature. However, in the temperature range close to room temperature, the effective stress for the deformation is quite sensitive to temperature. At the elevated temperatures (673~973 K) τ^* is relatively insensitive to the temperature.

5 DISCUSSION

The previous observations have indicated that both the data of activation parameters and the temperature dependence of yield stress can be classified into three temperature catalogs. In the temperature range close to room temperature the yield stress and deformation behavior is a slightly thermal activation behavior. At the elevated temperatures the yield stress and deformation behavior is rather athermal while it is obvious that the thermal activation behavior in the temperature range is higher than at the transition temperature. In addition, two transition temperature ranges occur among these three temperature catalogs.

In the low temperature catalog (298~398 K) the calculation indicates that the effective volume is smaller and the effective stress is larger. The large effective stress implies that the short-range resistance to the moving dislocations are large, which is overcome by the effective stress. The small value of effective volume means a short slip distance of the moving dislocations. The observations of the dislocation arrangement of deformed specimens at room temperature^[13] indicates that the main moving dislocation is the ordinary dislocation 1/2 (110], but the fraction of moving superdislocations including $1/2 \langle 101 \rangle$ and $1/2 \langle 112 \rangle$ is high up to 30%. The $1/2\langle 110|$ screw dislocations, which are arrayed in the long straight morphology, are dominant in the dislocation substructures. The 1/2 (110) dislocations are always pinned as shown in Fig. 4(a) while many superdislocations shown in Fig. 4(b) are faulted dipoles that have been proved to be formed by pinning of a partial dislocation. The closely pinning points along the dislocation lines imply very high P -N stress being present at the screw components^[14] and very low mobility of ordinary dislocations. Therefore, the effective stress needed to overcome the pinning should be large, and the activation volume is small. The pinned screw ordinary dislocations can glide by a mechanism of thermal activation movement of kinks or/ and jogs, which can be produced by colliding kink pairs on different slip planes. The thermal activation formation or movement of kinks or/ and jogs determines the moving rate of pinned dislocations. Therefore, the yield stress and deformation behavior in the temperature range close to room temperature exhibits a slightly thermal activation behavior. With increasing temperature both the yield strength and effective stress decrease. With increasing strain rate both the vield strength and effective stress increase. In general, the pinning of dislocations in TiAl is related to the asymmetrical bounding of Y-TiAl lattice as well as the sessile dissociation with faults. However, the high Nb content in the alloy may intensify the Peierls valleys and the asymmetrical bounding.

In the elevated temperature range (673~823

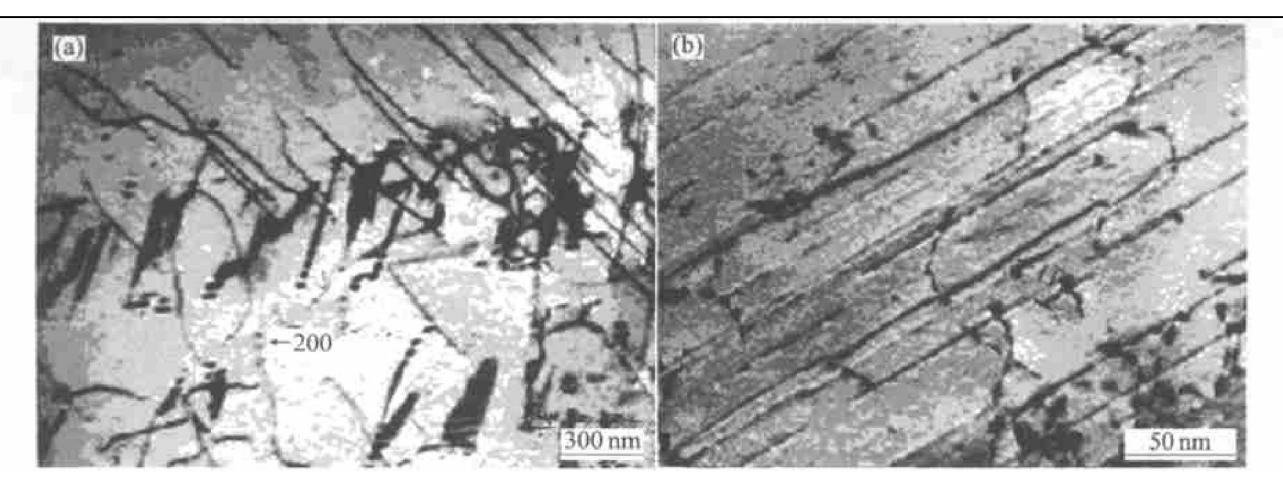


Fig. 4 Substructures of dislocations and faulted dipoles of Ti45Al10Nb alloy

K) the deformation behavior has been changed. The thermal activation analysis illustrates that the effective stress becomes smaller while the effective volume becomes larger. Therefore, the deformation behavior appears rather athermal. The slip resistance to moving dislocation mainly comes from the long-range resisting stresses of 220~ 230 MPa, which mainly include the elastic stress field of dislocation forest as well as the obstacles from interfaces and perhaps α_2 phase. Therefore both the long-range resisting stress and the yield stress decrease slowly corresponding to the temperature dependence on the shear modules. However, as the temperature rises to high enough the fault can move to the lower fault energy plane (similar to K-W mechanism, as an example), resulting in the difficulty of dislocation movement. While the cross slip can take place and then the dislocations pile up mainly on the grain boundaries, resulting in the grain boundary fracture started from the temperature near transition temperature.

For the high temperature deformation (> 1 088 K) the dislocation observations shown in Fig. 5 illustrate a completely different deformation behavior, corresponding to the strong thermal activation and temperature dependence of the yield strength. The apparent activation energy of high temperature deformation is estimated to be 3.66 eV, which is similar to the self-diffusion coefficient of TiAl. The dislocation observations illustrate that twinning appears to be one of the principal modes as deformed at 900 °C. In the Y laths, deformation twinning dominates, as shown in Fig. 5(a). The second principal deformation mechanism is the activity of ordinary dislocations shown in Fig. 5(b). The dislocations are generally curved or bowed. Trace analyses indicate that most of the segments glide on (111) plane, and their line directions change from 30° to edge orientation; but some of the segments near the pinning points do not lie on the rational planes. Especially, helical-shaped dislocations are observed such as the dislocations A and B in Fig. 5 (b). The segments making up the irregular helices lie on irrational planes like (441) and (332). The presence of many slip planes with little physical meaning seems to suggest that climb of ordinary dislocations has greatly contributed to plastic deformation. Superdislocations were further observed to be active simultaneously with ordinary dislocations as shown in Fig. 5(c); but faulted dipoles were not observed. These superdislocations have subjected to dissociation, as demonstrated in Fig. 5(d). Detailed analyses suggested that the dissociation of dislocations A is of the type: [011] = 1/6[154] + SISF+ 1/6[112].

From the measurement of the small radii of curvature ($R \sim 75$ nm) of the ordinary dislocation loops, the approximate shear stress needed to propagate the loop at room temperature was estimated by equation T = 14b/R to be 260 MPa. This calculated value of shear stress for ordinary slip is much higher than the value of $50 \sim 100$ MPa for normal Y phase. Similarly, the CRSS for ordinary dislocation slip at 1 173 K is estimated to be 180 MPa, from small radii of curvature of the ordinary dislocation loops. The increase of the CRSS for ordinary slip in Y phase by a high-Nb solution is further confirmed at high temperatures.

6 CONCLUSIONS

- 1) In the temperature range close to room temperature the yield stress and deformation behavior exhibits a slightly thermal activation behavior. The thermal activation formation of kinks or/ and jogs determines the moving rate of pinned dislocations. The CRSS for ordinary dislocation slip at room temperature is estimated to be of ~ 260 MPa.
- 2) In the elevated temperature range ($673 \sim 823$ K), the effective stress becomes smaller while

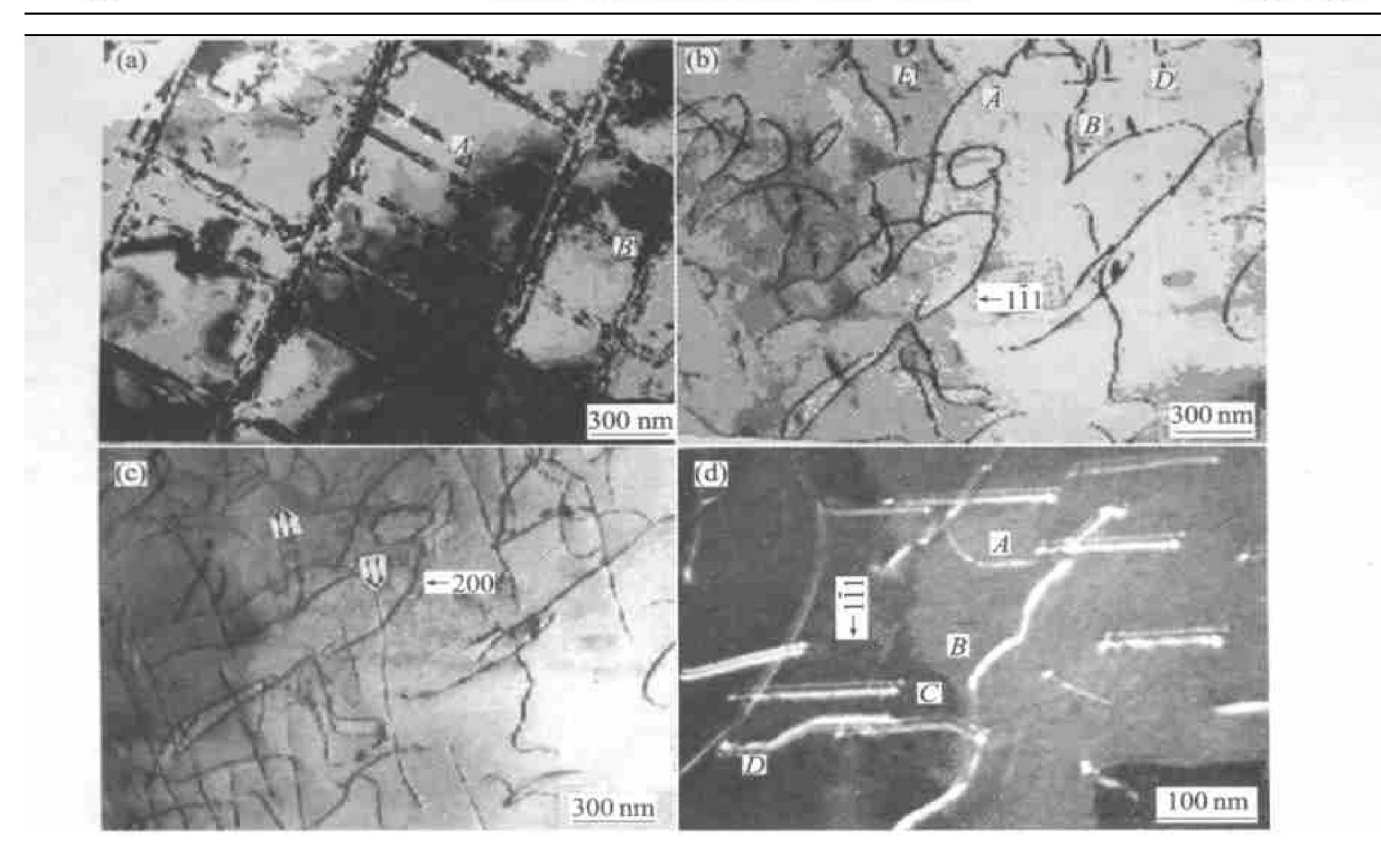


Fig. 5 Superdislocation substructures of Ti45Al10Nb alloy deformed at high temperature

the effective volume becomes larger. Therefore, the deformation behavior appears rather athermal.

- 3) The data of ΔG in the high temperature range is very high, corresponding to the strong temperature dependence of the yield strength. The apparent activation energy of high temperature deformation is estimated to be 3. 66 eV, which is larger than the self-diffusion coefficient of binary TiAl (3.01 eV).
- 4) The effective stresses at room temperature for the high Nb containing TiAl alloy is larger than that with low Nb content. The climb rate of dislocation may be also reduced by high Nb content, resulting in a higher CRSS of moving dislocation.

[REFERENCES]

- [1] Kim Y W. Effects of microstructure on the deformation and fracture of FTiAl alloys [J]. Mater Sci and Eng, 1995, A192/193: 519.
- [2] Huang S C. Alloying condensation in gamma based alloys [A]. Darolia R, Lewandowski J J, Liu C L. Structural Intermetallis [C]. TMS, 1993. 299.
- [3] Appel F, Wagner R. Deformation mechanisms in TiAl/ Ti₃Al structures [A]. Kim Y W, Wagner R, Yamaguchi M. Gamma Titanium Aluminides [C]. TMS, 1995. 231.
- [4] Lin D L, Wang Y, Law C C. Thermal activation processes of tensile deformation in Y-TiAl alloy[J]. Mater Sci Eng, 1997, A239/240: 369.
- [5] Kim Y W. Trends in the development of gamma TiAl alloys
 [A] . Kim Y W, Wagner R, Yamaguchi M. Gamma Titar

- nium Aluminides [C]. TMS, 1995. 637.
- [6] CHEN G, SUN Z, ZHOU X. Oxidation of intermetallic alloys in Nb Tr Al ternary system [J]. The J of Sci Eng Corrosion, 1992, 48(11): 939 946.
- [7] CHEN G, ZHANG W, WANG Y, et al. TrAl-Nb intermetallic alloys based on the ternary intermetallic compound [A]. Darolia R. Structural Intermetallics[C]. TMS Publication, 1993. 319.
- [8] ZHANG W, CHEN G, WANG Y. Oxidation of ternary Ti18Nb48Al and Ti10Nb45Al[J]. Scripta Met, 1993, 28 (5): 563.
- [9] Schock G. Thermodynamics and thermal activation of dislocations [A]. Nabarro F R N. Dislocations in Solids [C]. Vol. 10. 63.
- [10] Liu C T, Maziasz P J, Wright J L. Microstructural control and mechanical properties of dual-phase TiAl alloys [J]. Intermetallics, 1998, 6: 653.
- [11] Surek T, Luton M J, Jonas J J. Dislocation glide controlled by linear elastic obstacles: a thermodynamic analysis [J]. Philos Mag, 1974, 69A: 425.
- [12] Kim Y W. Designing gamma TiAl alloys: fundamentals, strategy and production[A]. Nathal M V, Darolia R, Liu C T. Structural Intermetallics[C]. TMS, 1997. 531.
- [13] ZHANG W J, LIU Z C, CHEN G L. Dislocation structure in a Tr 45% Al 10% Nb alloy deformed at room temperature [J]. Phil Mag A, 1999, 79(5):1073.
- [14] Greenberg B A, Antonova O V, Indenbaum V N. Dislocation transformations and the anomalies of deformation characteristics in TiAl—I. Models of dislocation blocking [J]. Acta Metall Mater, 1991, 39(2): 233.

(Edited by PENG Chao gun)